Volume 18 | Number 11 | 21 March 2016 | Pages 7541–8248

PCCP

Physical Chemistry Chemical Physics

www.rsc.org/pccp

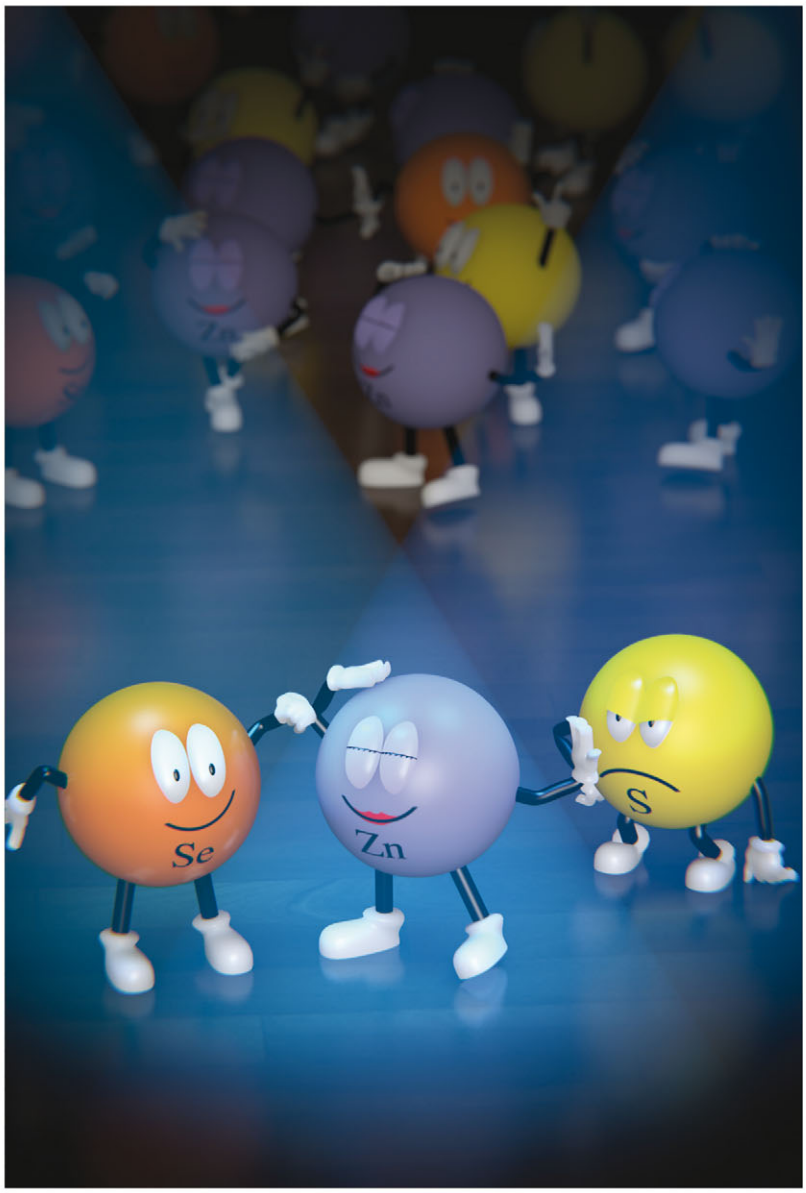

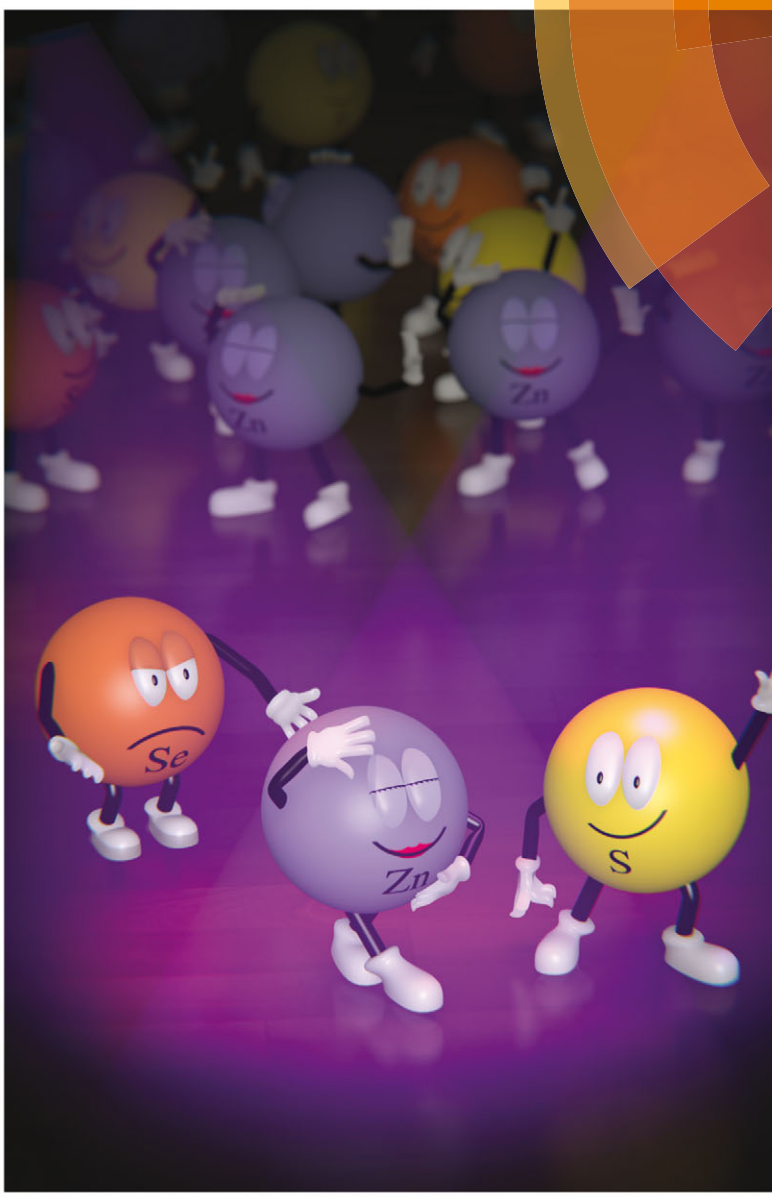

ISSN 1463-9076

ROYAL SOCIETY OF CHEMISTRY

PAPER

M. Dimitrievska, V. Izquierdo-Roca *et al.*

Resonant Raman scattering of ZnS_xSe_{1-x} solid solutions: the role of S and Se electronic states

175 YEARS

PCCP

PAPER

View Article Online
View Journal | View Issue

Cite this: *Phys. Chem. Chem. Phys.*, 2016, **18**, 7632

Resonant Raman scattering of ZnS_xSe_{1-x} solid solutions: the role of S and Se electronic states

M. Dimitrievska,*[a] H. Xie,[a] A. J. Jackson,[b] X. Fontané,[a] M. Espíndola-Rodríguez,[a] E. Saucedo,[a] A. Pérez-Rodríguez,[ac] A. Walsh[b] and V. Izquierdo-Roca*[a]

Received 30th July 2015,
Accepted 27th August 2015

DOI: 10.1039/c5cp04498g

www.rsc.org/pccp

A comprehensive Raman resonance scattering study of ZnS_xSe_{1-x} (ZnSSe) solid solutions over the whole compositional range ($0 \leq x \leq 1$) has been carried out using 325 and 455 nm excitation wavelengths. The Raman scattering intensities of LO ZnS-like and ZnSe-like phonon modes, corresponding to pure S and Se vibrations, respectively, are revealed to be significantly enhanced when excited with 325 nm excitation in the case of S vibrations, and with 455 nm in the case of Se vibrations. This behavior is explained by the interaction of the excitation photons with the corresponding S or Se electronic states in the conduction band, and further confirmed by first principles simulations. These findings advance the fundamental understanding of the coupling between the electronic transitions and photons in the case of Raman resonance effects, and provide inputs for further studies of lattice dynamics, especially in the case of chalcogenide materials. Additionally, the coexistence of modes corresponding to only S vibrations and only Se vibrations in the ZnSSe alloys makes these results applicable for the compositional assessment of ZnSSe compounds.

Introduction

Wide band gap II–IV semiconductor binaries and their solid solutions have gained considerable attention due to their potential application in electronic and optoelectronic devices. The efficient miscibility of ZnS and ZnSe compounds in the ZnS_xSe_{1-x} (ZnSSe) solid solutions over the whole compositional range, $0 \leq x \leq 1$, enables easy tuning of the band gap energies (ranging from 2.67 eV (ZnSe) to 3.66 eV (ZnS)) and the lattice constants, which additionally enhances the potential application of these materials. ZnSSe compounds have been reported as highly suitable and promising materials for blue lasers, light emitting diodes, light emitters, and wavelength tunable UV photodetectors, due to their wide direct band gap and high photoresistivity.[1–4] Polycrystalline ZnSSe compounds are excellent candidates for window and/or buffer layers in thin film heterojunction solar cells and promising alternatives to the presently explored materials such as CdS, which contain toxic Cd.[5,6] Additionally, because of its low absorption at infrared wavelength and exciton binding energy, ZnSSe is considered as a future material in the production of biomedical labels, output couplers, lenses, and optically controlled switches. Changing the ratio of S to Se of ZnSSe compounds leads to tuning of the electron affinity and electrical properties which greatly enhances the blue response of the material.[7] ZnSSe may also appear as a secondary phase in other multinary compounds, like $Cu_2ZnSn(S,Se)_4$, which have shown promising results for application as thin film absorber layers in solar cells.[8,9] It has been shown that ZnSSe secondary phases, besides having unfavorable effects on the conversion efficiency of solar cells, are also quite challenging for detection using standard characterization techniques such as X-ray diffraction (XRD). For all these reasons, synthesis and characterization of ZnSSe materials is a very attractive topic.

Until now, a wide range of characterization studies on the ZnSSe thin films have been reported, including structural, electrical and optical property variations depending on the S/Se ratio.[2,5,7,10–16] Raman spectroscopy as such has been extensively used for investigating the lattice vibration dynamics in these systems.[12,14,17,18] Raman scattering is a powerful non-destructive method which can provide useful information on the structure, morphology and chemical composition of semiconductor materials, as well as on the photon–electron and electron–phonon interactions occurring in these materials. Although many studies have been devoted to compositional dependence of the optical modes in the ZnSSe systems, most are usually done using standard non-resonant Raman conditions. The main disadvantage of the standard excitation methods is the observation of high number of Raman modes with relatively low intensity, which leads to difficulties in the determination of peak

[a] *Catalonia Institute for Energy Research (IREC), Jardins de les Dones de Negre 1, 08930 Sant Adrià de Besòs, Spain. E-mail: mdimitrievska@irec.cat, vizquierdo@irec.cat*
[b] *Centre for Sustainable Chemical Technologies and Department of Chemistry, University of Bath, Claverton Down, Bath BA2 7AY, UK*
[c] *IN²UB, University of Barcelona, C. Martí Franquès 1, 08028 Barcelona, Spain*

positions and phase identification. This is due to very weak Raman scattering efficiency of ZnSSe compounds caused by weak photon–matter interaction under standard excitations (514 and 532 nm lasers).[19,20] In contrast, resonance Raman methods allow measuring spectra, which are simpler in the sense that the number of observed independent modes is lower and at the same time, with several orders of magnitude higher intensity.[20–22] This allows easier identification of the modes and facilitates their correlation with other properties, such as composition, impurities, defects, crystallinity, and electronic band structure. Additionally, the use of resonant Raman conditions allows the use of shorter integration times, usually of the order of seconds, which is a significant advantage when compared to other characterization methods, especially in the case of nanosystems, where normally long integration times are required for the structural and electrical characterization.

In this work a study of the vibrational properties of ZnSSe solid solutions, over the full range of anion compositions, $0 \leq [S]/([S] + [Se]) \leq 1$, was made using resonance Raman spectroscopy. A special focus is put on the changes in the integral intensity of the Raman modes sensitive to anion vibrations, with the variations in the excitation energy. It is observed that Raman modes corresponding to S vibrations are exhibiting resonance behavior in the case of 325 nm excitation, while Raman modes corresponding to Se vibrations become resonant when probed with 455 nm excitation. This behavior is explained by the interaction of the excitation photons with the corresponding S or Se states in the electronic band structure, and confirmed by first principles calculations. The understanding of this kind of resonance effect could improve fundamental knowledge not only of the ZnSSe compounds, but also other types of mixed chalcogenide materials, including Cd-(S,Se) and Mo-$(S,Se)_2$. Finally, these results can be applied for the development of a simple and non-destructive optical methodology for the quantitative measurement of [S]/([S] + [Se]) anion composition in ZnSSe solid solutions by means of Raman spectroscopy.

Experimental

Thin film formation

Zn precursors of 80 nm were deposited by DC-magnetron sputtering (Ac450 Alliance Concepts) using a power density of 1.27 W cm^{-2} onto glass substrates. Binary ZnS thin films were produced by reactive annealing of the Zn precursors under a sulfur atmosphere at 550 °C, 1 bar Ar pressure for 30 min, and using a crucible with 50 mg of sulfur powder (Alfa-Aesar, 99.995%). ZnSe thin films were produced by reactive annealing under a selenium atmosphere at 550 °C for 30 min with the flow of Ar to maintain a pressure of 1 mbar, and with a crucible containing 50 mg of selenium powder (Alfa-Aesar, 99.999%). To form ZnSSe alloy films a single-step sulfo-selenization annealing was used.[8] This process is similar to that used for the pure ZnS or ZnSe films, but varying the ratio of the mixture of sulfur and selenium while maintaining the total weight of the mixture of 50 mg. Two annealing temperature profiles were employed; "one step profile": 550 °C, 30 min, and 1 mbar or 1 bar; and "two step profile": first 200 °C in 1 mbar atmosphere and then 550 °C for 30 min in 1 bar atmosphere, which is proved to be beneficial for obtaining various Se-rich thin films. The heating rate for all thermal treatments was 20 °C min^{-1} and the cooling process was allowed to proceed naturally.

Characterization

Raman scattering measurements were performed in back scattering configuration using a LabRam HR800-UV and DXR™xi Raman Imaging Microscope. For the HR800-UV system, a gas HeCd laser with a wavelength of 325 nm was used for excitation. In this system excitation and light collection were made using an Olympus metallographic microscope with a laser spot diameter of the order of 1–2 μm. To avoid effects in the spectra related to potential microscopic inhomogeneities, the spot was rastered over an area of 30 × 30 μm^2. Furthermore, the DXR™xi Raman Imaging Microscope system works coupled with a 455 nm laser, with a 1–2 μm diameter spot size on the sample. In all cases, and to avoid the presence of thermal effects in the spectra, the power excitation density on the surface of the samples was around 50 W cm^{-2}. Under these experimental measurement conditions no thermal effects are observed in the spectra. This has been corroborated by the analysis of spectra measured with different excitation powers. The first-order Raman spectrum of monocrystalline Si was measured as a reference before and after acquisition of each Raman spectrum, and the spectra were corrected with respect to the Si line at 520 cm^{-1}.

XRD patterns were measured on a Siemens D500 diffractometer with Cu-Kα-radiation (λ = 1.54056 Å) in a θ–2θ configuration. Refinements of the lattice constant values were carried out by Le Bail analysis using the FullProf package.[23]

The band gap energies were determined from the ultraviolet-visible (UV-Vis) spectra which were obtained using a Perkin Elmer Lambda 950 UV/VIS spectrometer.

The composition of the samples was measured using X-ray fluorescence (XRF) spectroscopy performed on a Fisherscope XVD system.

The synthesized films have been imaged by scanning electron microscopy (SEM) using a ZEISS Series Auriga microscope with 5 kV acceleration voltage.

Theoretical calculations

Electronic structure calculations within density functional theory (DFT) were carried out within periodic boundary conditions as implemented in VASP, a quantum chemistry package using plane-wave basis sets.[24] 8-atom unit cells were formed for ZnS, a ZnSSe alloy with 3 : 1 S : Se ratio, and ZnSe (Fig. 1). The alloy cell of composition Zn_4S_3Se provides a mixture of Zn–S and Zn–Se interactions for comparison with the binary compounds; however, the effects of long-range disorder are neglected in this work. The initial lattice parameters were a = 5.383 Å for ZnS and the alloy cell, and a = 5.667 Å for ZnSe, based on crystallographic studies;[25,26] these structures were optimized with the PBEsol exchange–correlation functional, using projector-augmented wave (PAW) pseudopotentials optimized for the PBE functional

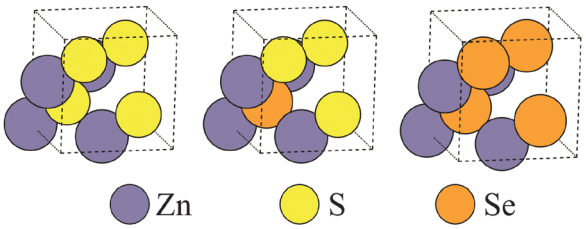

Fig. 1 Unit cells for theoretical calculations. Zn (indigo), S (yellow) and Se (orange) atoms in 8-atom ZnS (a = 5.363 Å), alloy (a = 5.431 Å) and ZnSe (a = 5.642 Å) unit cells.

and including the Zn 3d states as valence electrons. The basis-set energy cutoff was 500 eV and the Brillouin zone was sampled with a 5 × 5 × 5 Γ-centered k-point grid (reduced by symmetry to 10 irreducible points).[27] The ionic positions and lattice parameters were optimized by a succession of conjugate gradient procedures until the difference in total energy between relaxation steps was reduced to below 1 meV. The structures optimized with PBEsol were then used for electronic structure calculations with the non-local screened hybrid HSE06 exchange–correlation functional.[28] The same pseudopotentials and energy cutoff were used for these calculations, while the k-point mesh density was increased to 15 × 15 × 15 (reduced by symmetry to 120 points). In these cases the initial electronic structure convergence was achieved by Gaussian smearing (σ = 0.05 eV), and the density of states was refined by further SCF iterations using the tetrahedron method with Blöchl corrections.

Results and discussion

The crystal structure of ZnSSe solid solutions was characterized by XRD measurements from which representative patterns are presented in Fig. 2(a). All main diffraction peaks have been identified for the zinc-blende structure,[29] and no evidence of any other phases or impurities has been found. Furthermore, the presence of a single and symmetric (111) diffraction peak in all measured patterns implies that all samples are homogeneously alloyed rather than a mixture of ZnS and ZnSe phases. The systematic shift in peak positions toward higher angles as the [S]/([S] + [Se]) ratio increases correlates with the replacement of smaller S atoms with larger Se atoms, which in turn leads to a decrease in the lattice constants. The lattice constants of the ZnSSe solid solutions were obtained as a result of the Le Bail analysis, for which the zinc-blende structure was used as a starting model for the refinements. By assuming the validity of Vegard's law and using the lattice constants calculated from the XRD data, the anion compositions [S]/([S] + [Se]) of the ZnSSe thin films were determined and are presented in Fig. 2(b). The obtained results are in agreement with the previously reported data.[13,30–32]

The band gap energies of the ZnSSe compounds have been evaluated from the UV-vis absorption spectra using the Tauc relation:[33]

$$(\alpha h\nu)^n = C(E - E_g) \quad (1)$$

where α is the absorption coefficient, h is Planck's constant, ν is the frequency, n = 2 for a direct band gap semiconductor material (such as ZnSSe), C is a proportionality constant, E is the energy (equal to $h\nu$), and E_g is the band gap energy. The estimated band gap energies for each anion composition of the ZnSSe alloys are shown in Fig. 2(b). It is observed that the band gap energies can be tuned from 3.66 eV in pure ZnS thin films to 2.67 eV in pure ZnSe thin films, just by changing the anion composition in the samples. The change in the band gap energies with the anion composition x = [S]/([S] + [Se]) shows nonlinear behavior and can be fitted as a quadratic function of x:

$$E_g(x) = xE_g(\mathrm{ZnS}) + (1 - x)E_g(\mathrm{ZnS}) - x(1 - x)b \quad (2)$$

where E_g(ZnSe), E_g(ZnS), and $E_g(x)$ are the band gap energies of ZnS, ZnSe, and their alloy, respectively, while b is the bowing constant, and in this case the best fit was obtained for b = 0.70(6), which is in agreement with the previously reported values.[34]

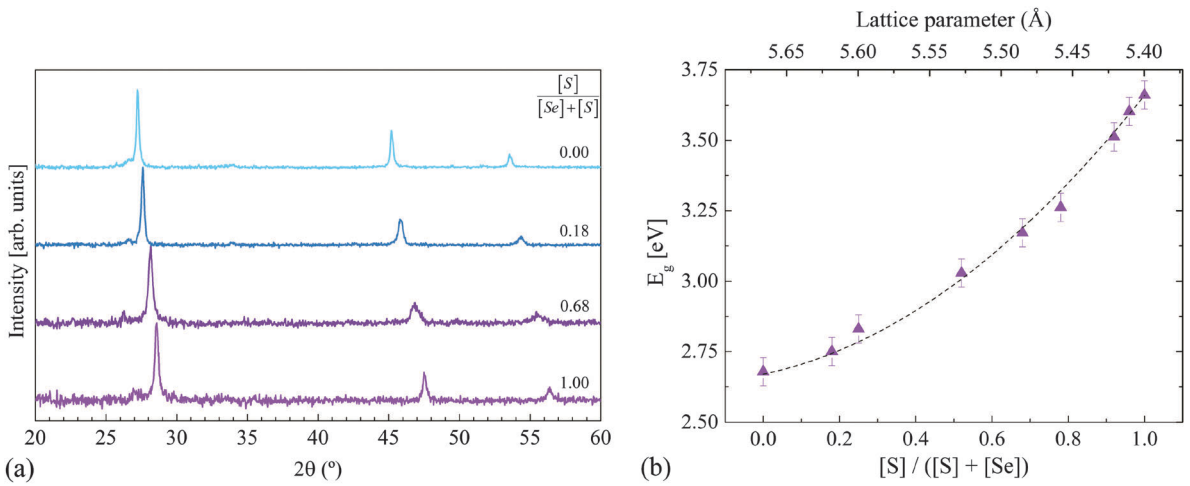

Fig. 2 (a) Representative XRD patterns of ZnSSe solid solutions for different anion compositions and (b) band gap energies depending on [S]/([S] + [Se]) compositions and lattice constants.

The Raman scattering spectra of ZnSSe solid solutions measured under ultra-violet (UV) (λ = 325 nm, 3.82 eV) and blue (λ = 455 nm, 2.72 eV) excitations are shown in Fig. 3. Raman spectra of the pure ZnS measured under resonant conditions (UV excitation) are characterized by the strongly enhanced longitudinal optical (LO) phonon mode observed at 348 cm^{-1}.[20] This mode is attributed to vibrations

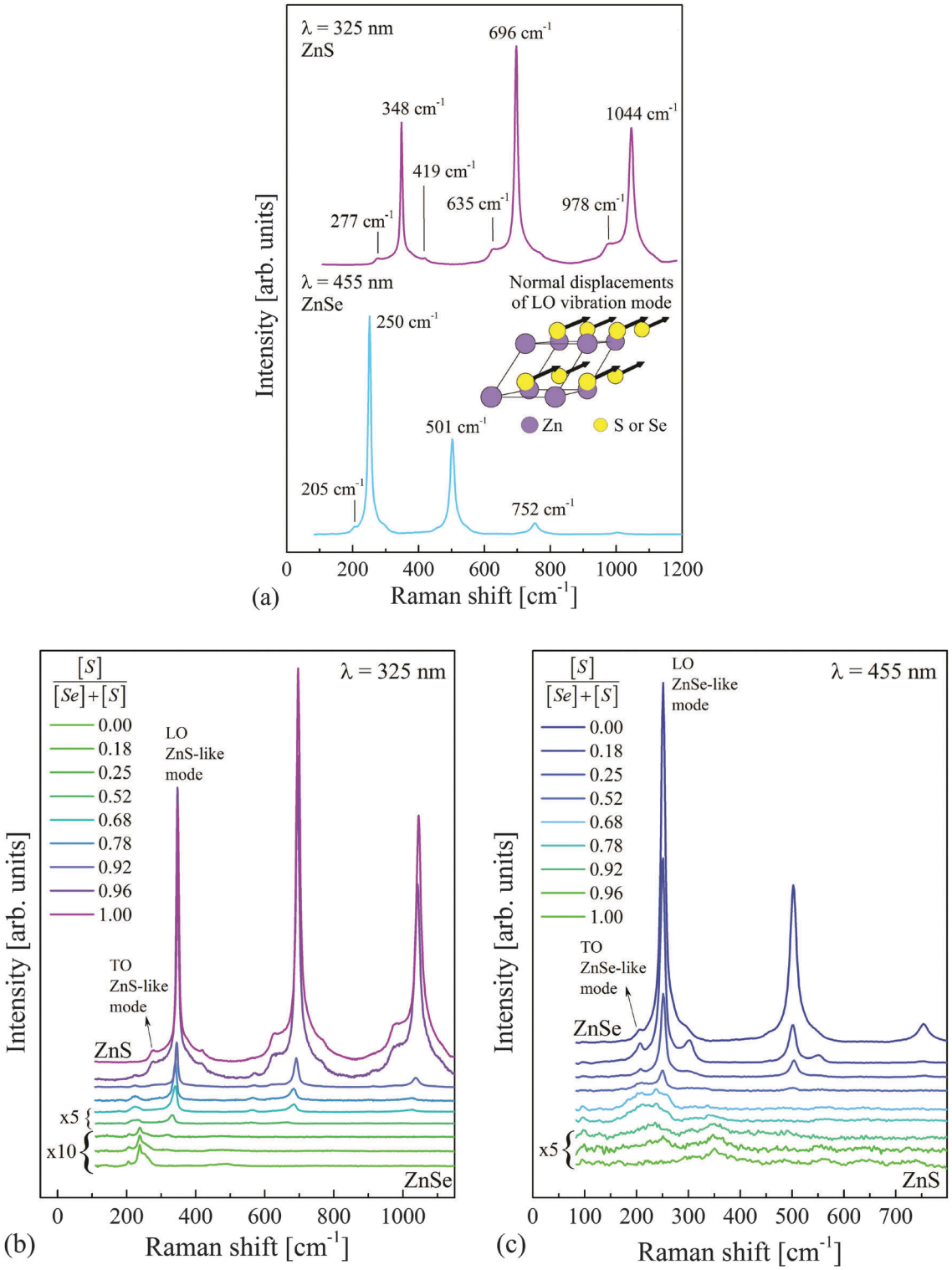

Fig. 3 (a) Normalized reference Raman spectra of pure ZnS and ZnSe compounds with the identification of modes measured under resonant conditions; the inset shows the normal displacements of the LO phonon mode for pure ZnS or ZnSe, with the arrows indicating the direction of the movement of the atoms; (b) and (c) Raman spectra of ZnSSe solid solutions measured with 325 and 455 nm excitation wavelengths. Some of the low intensity spectra in both cases were multiplied ×5 or ×10 for more details, as labeled in the figure.

of only S anions in the lattice. An illustration of the normal displacements of the LO phonon mode, obtained from the first principles simulations, is presented in the inset of Fig. 3(a). Second (LO2) and third (LO3) orders of this mode are also observed at 696 and 1044 cm^{-1} frequencies, respectively. Additionally, a lower intensity peak is observed at 277 cm^{-1}, and attributed to the fundamental transverse optical (TO) phonon mode. Bands at 419, 635 and 978 cm^{-1} are attributed to the higher order combination bands of the fundamental modes.[35] In the case of pure ZnSe, a resonance Raman spectrum is measured under the blue excitation, and characterized by the strongly enhanced LO mode at 250 cm^{-1}, attributed to vibrations of only Se anions, and a low intensity TO mode observed at 205 cm^{-1}.[36] Again, second (LO2) and third (LO3) order peaks are observed at 501 and 752 cm^{-1}, respectively. The first order Raman spectra of ZSSe solid solutions are characterized by the presence of two dominant peaks in the frequency region 270–350 cm^{-1}, and two dominant peaks in the frequency region 200–270 cm^{-1}. The peaks in the higher frequency region are identified as ZnS-like peaks corresponding to TO and LO phonon modes involving S vibrations, and the peaks in the lower frequency region are identified as ZnSe-like peaks corresponding to TO and LO phonon modes involving Se vibrations.[37,38] This agrees with the existence of a two-mode behavior of these peaks, as previously reported.[17,37,39,40]

The optical phonon frequencies vary with the changes in composition. With the increase in S composition, the LO ZnSe-like peak shifts downward in frequency, while the TO ZnSe-like peak monotonically moves upward. For the very S-rich samples, these two modes almost overlap, and then finally disappear for $x = 1$. Similar behavior is observed for the LO and TO ZnS-like peaks with the increase in the Se composition. The compositional dependence of LO and TO frequencies for both ZnS-like and ZnSe-like peaks is shown in Fig. 4. Solid lines in Fig. 4 present the calculated phonon frequencies of the modes using the modified-random-element-isodisplacement (MREI) model.[17] Additional information about the MREI model, as well as the explanation of the calculation process and the parameter values used for obtaining results presented in Fig. 4, is given in ref. 17. The experimental data presented in Fig. 4 are in good agreement with the model predictions and as well as the previously reported results.[39,40]

Asymmetrical broadening in the low frequency side of the LO ZnS-like peak can be observed with the decrease in the S composition in the Raman spectra measured with 325 nm excitation. Similarly, asymmetrical broadening in a low frequency side of the LO ZnSe-like peak is noticeable in the Raman spectra measured with 455 nm excitation, with the decrease in Se composition. This phenomenon is attributed to the phonon confinement effects arising from the loss of translational symmetry in the crystal caused by the alloy disorder.[39–41]

An interesting phenomenon, which was not previously observed in the ZnSSe systems, is the intensity dependence of the LO ZnS-like and LO ZnSe-like modes with the excitation energy. Fig. 5(a) and (b) present the changes in the intensity of the LO ZnS-like and ZnSe-like modes with respect to the

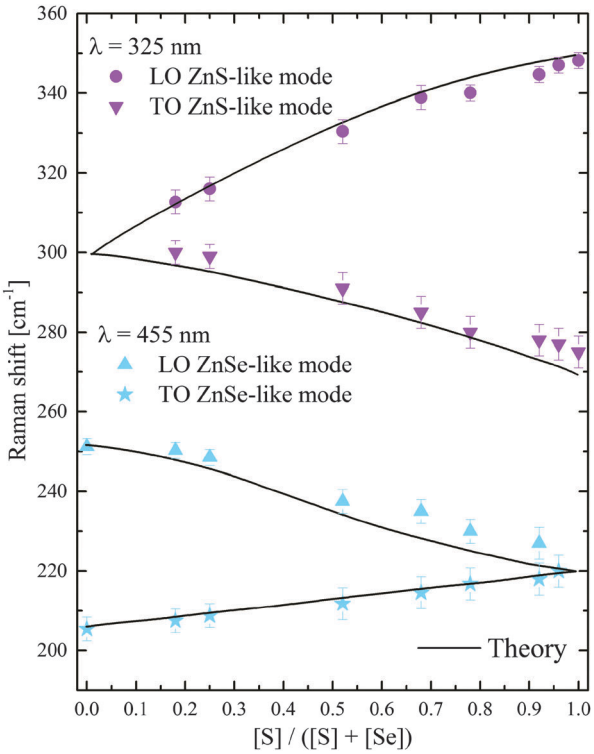

Fig. 4 The optical phonon frequencies of the ZnSe-like and ZnS-like modes as a function of the anion composition [S]/([S] + [Se]). The ZnSe-like and ZnS-like mode frequencies were determined from the resonance Raman spectra measured with 455 and 325 nm excitation wavelength, respectively. The solid lines represent the theoretical frequencies obtained by the modified random-element-isodisplacement model.

difference between the energy band gap and the excitation energy.

Three kinds of resonance behaviors can be observed from the results presented in Fig. 5. In the case of S-rich ZnSSe samples, only LO ZnS-like peaks are enhanced when measured with UV excitation; while LO ZnSe-like peaks do not exhibit resonance behavior for any of the used excitation wavelengths. A reverse situation is observed for the Se-rich ZnSSe samples, where LO ZnSe-peaks are enhanced in the Raman spectra measured with blue excitation; while LO ZnS-like peaks show non-resonance behavior for any of the used excitation wavelengths. Lastly, for the case of intermediate anion compositions, the LO ZnS-like peaks become resonant when using the UV excitation and the LO ZnSe-like peaks become resonant when probed using the blue excitation.

According to these experimental results, UV excitation only enhances modes correlated with vibrations of S anions, while blue excitation only induces resonance effects in modes attributed to vibrations of Se anions. This behavior suggests that UV photons mostly interact with S electronic states, while blue photons interact with Se states. Further explanation of these results can be made by taking into account the electronic band structure of ZnSSe compounds and working principles of the resonance Raman effect.

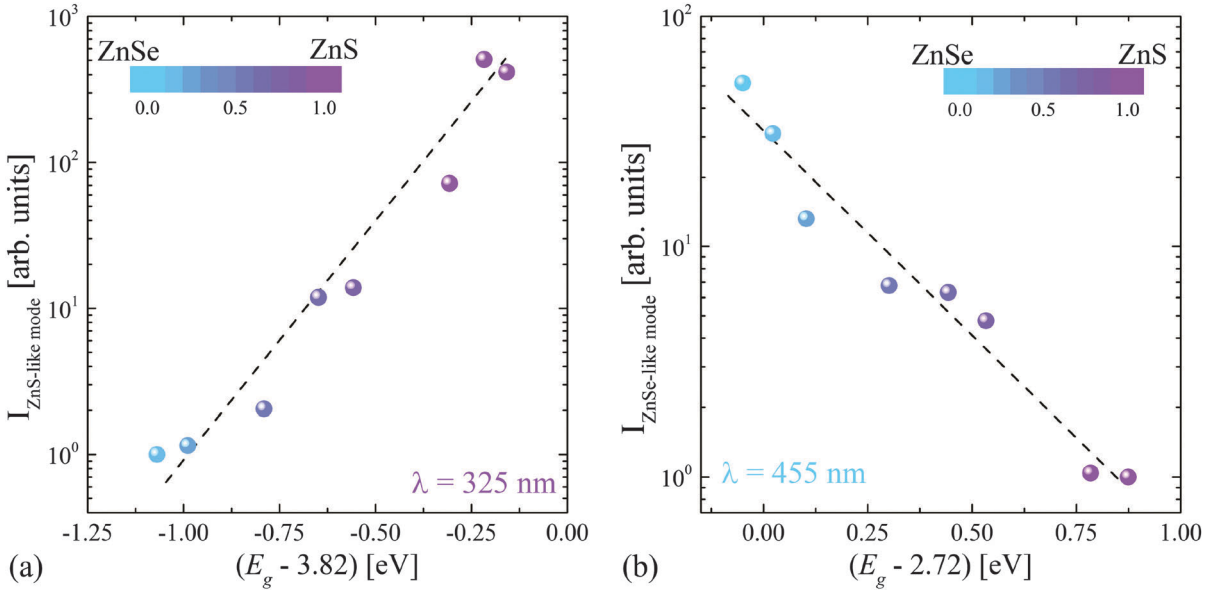

Fig. 5 Enhancement in the intensity of the (a) LO ZnS-like mode and (b) LO ZnSe-like mode depending on the difference between the band gap energy of the ZnSSe thin films and the excitation energy. Dashed lines are a guide to the eye.

In general, Raman scattering intensity can be defined as:[42,43]

$$I(\omega_i) \propto {\omega_s}^4 |\hat{e}_s \cdot R \cdot \hat{e}_i|^2 \left| \sum_{\alpha\beta} \frac{1}{(E_\alpha - \hbar\omega_i - i\Gamma_\alpha)(E_\beta - \hbar\omega_s - i\Gamma_\beta)} \right|^2 \quad (3)$$

where ω_s and ω_i are the scattered and the incoming photon frequencies, respectively; E_α and E_β are the energies of the intermediate crystal states, R is the Raman tensor, $\hat{e}_s$ and $\hat{e}_i$ are the scattered and the incident polarization vectors, and Γ_α and Γ_β are damping constants. The first term in eqn (3) represents the dipole transition radiation; the second term represents the Raman selection rules, which is dependent on the crystal symmetry, while the last term represents the resonance effects. As the incident excitation energy is tuned to the energy of the intermediate state, the denominator in eqn (3) becomes smaller, which then leads to the enhancement in the Raman intensity, and thus the resonance effects. Raman resonance effects in semiconductors may be achieved if the excitation energy approaches the band-gap energy, or *via* the interaction of the incident photon with the exciton states or the impurity states.

For the pure ZnS and ZnSe compounds, the energies of the above-gap S and Se states are close to the energy band gap, which are 3.66 and 2.82 eV, respectively.[44] As the energy of the S states is close to the energy of the UV photons (3.82 eV or 325 nm), the interaction between them will result in a decrease in the denominator value in eqn (3), which will then lead to the increase in intensity of the Raman mode associated with this interaction (LO mode). This is why only LO modes will be enhanced in the Raman spectra of ZnS when measured with UV excitation. A similar situation is expected in the case of LO mode in pure ZnSe when probed with blue excitation (2.72 eV or 455 nm).

Previous studies of the electronic structure of Zn chalcogenides identified an increase in the valence band energy of ~0.5 eV between ZnS and ZnSe,[45,46] arising from the lower binding energy of the Se 4p states compared to S 3p. There is a comparable drop in the conduction band energy, due to the larger Zn–Se bond length compared to Zn–S, leading to an overall difference in E_g of ~1.0 eV. In the case of ZnSSe mixtures, both S and Se states are involved. Depending on the anion composition of the solid solution, the electronic density of states is expected to interpolate smoothly between those of the binary compounds.

For crystals with intermediate composition, changes in the S and Se electronic states are low enough to allow the preservation of the resonance excitation behavior of the LO ZnS-like and ZnSe-like modes with the UV and blue excitations, respectively. However, for S-rich or Se-rich alloys this is not the case. As an example of the last situation, Fig. 6 shows the full and species-projected density of states for ZnS, $ZnS_{0.75}Se_{0.25}$ and ZnSe. As can be seen in the case of $ZnS_{0.75}Se_{0.25}$, the above-gap S states are shifted slightly closer to the Fermi level in comparison to the pure ZnS compound, while the above-gap Se states are shifted considerably further from the Fermi level relative to the pure ZnSe compound.

This means that for S-rich ZnSSe samples, interaction between S states and UV photons is expected, due to their similar energies, while no interaction will occur between Se states and blue photons, because of their energy mismatch. This should then lead to resonance behavior of the LO ZnS-like modes, when probed with UV excitation, and non-resonance behavior of LO ZnSe-like modes when probed with blue excitation, which is experimentally observed. An opposite situation is expected in the case of Se-rich samples. Similar resonance effects were also observed in the case of kesterite solid solutions $Cu_2ZnSnS_xSe_{1-x}$.[47]

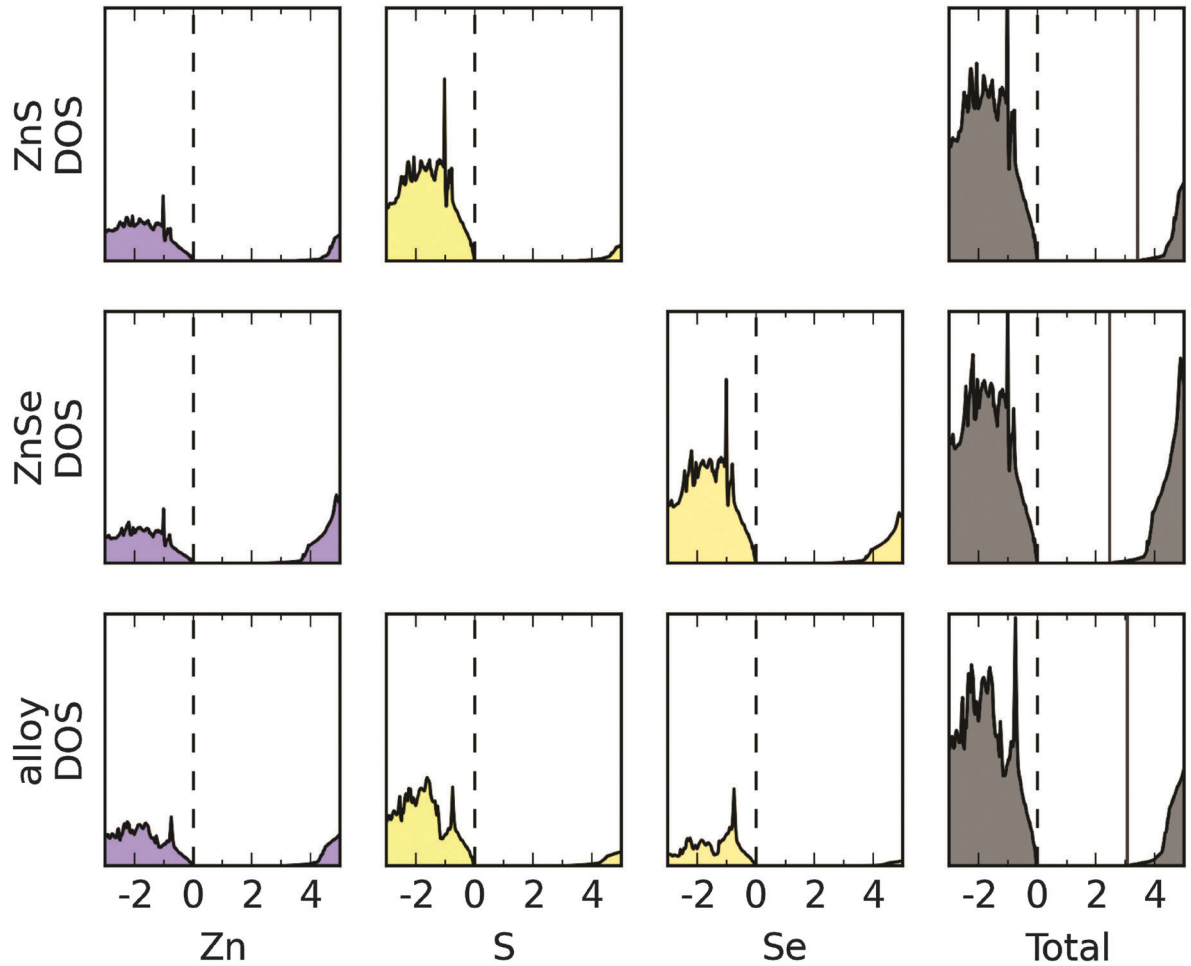

Fig. 6 Partial and total density of states (DOS) for ZnS, ZnSe and $ZnS_{0.75}Se_{0.25}$ alloys obtained from hybrid DFT calculations. Horizontal axes give energy relative to the Fermi level (indicated with a dashed line) in eV. The right-most column represents total DOS; the vertical solid line indicates the conduction band minimum (CBM).

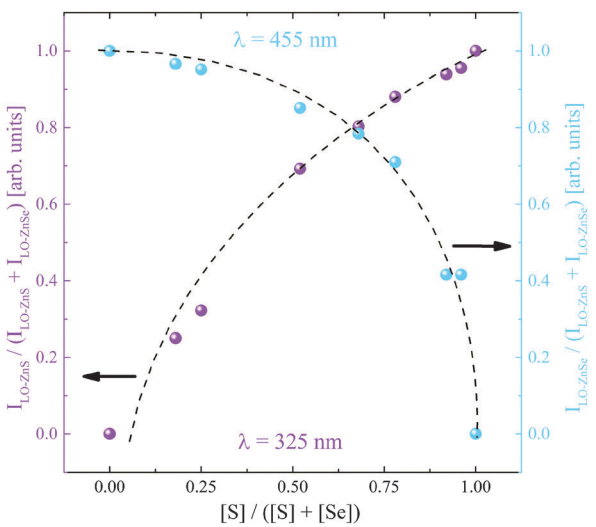

Fig. 7 Anion composition depending on the integral intensity ratio of LO ZnS-like and LO ZnSe-like peaks calculated from Raman spectra measured with 325 and 455 nm excitation.

Finally, these results can be applied for the development of a simple and non-destructive optical methodology for the quantitative measurement of [S]/([S] + [Se]) anion composition in ZnSSe solid solutions by means of Raman spectroscopy, similar to the study presented in ref. 48. Since the intensity of LO ZnS-like and ZnSe-like modes is proportional to the concentration of S and Se in the material, respectively, plotting the integral intensity ratio of these two bands *versus* the anion composition should give the calibration curves which can be later used for the estimation of anion composition in unknown ZnSSe samples. An example of this kind of plot is given in Fig. 7. As shown in the figure, for S-poor compositions changes in the relative intensity of the ZnS-like peak are very sensitive to changes in the alloy composition, while for S-rich compositions changes in the relative intensity of the ZnSe-like peak are very sensitive to changes in the alloy composition. In general, this methodology is completely independent of the experimental conditions of the measurements and of the type of sample, which is another advantage of using Raman spectroscopy for the estimation of the anion composition in this kind of material.

Conclusions

This work describes joint experimental and theoretical investigation of the Raman resonance effects in ZnSSe solid solutions. Resonance behavior is observed in the Raman modes corresponding to the anion vibrations, when changing the excitation energy from UV (325 nm) to blue (455 nm). Significant enhancement in the Raman intensity of the LO ZnS-like modes, corresponding to pure S vibrations, is observed in cases of S-rich and intermediate compositions when excited with UV energy. On the other side, LO ZnSe-like modes attributed to pure Se vibrations are enhanced in the case of blue excitation for samples with Se-rich and intermediate compositions. This enhancement of only certain Raman modes in the spectra is explained by interaction of the excitation photon with the corresponding S or Se states in the electronic band structure, and confirmed by the first principles calculations. Raman resonance effects in this case are achieved due to the tuning of the excitation energy with the energy of the S or Se electronic states in the conduction band. These findings advance the fundamental understanding of the coupling between the electronic transitions and photons in the case of Raman resonance effects, and provide inputs for further studies of lattice dynamics, especially in the case of chalcogenide materials. Additionally, the application of Raman resonant conditions in the case of this kind of material can be used for developing a simple and non-destructive optical methodology for the quantitative measurement of [S]/([S] + [Se]) anion composition. They should also enable easier characterization of the ZnSSe system, like reducing the integration time of the Raman measurements, which is extremely important in the case of nanosystems.

Acknowledgements

The research leading to these results has received funding from the People Program (Marie Curie Actions) of the European Union's Seventh Framework Program FP7/2007-2013/under REA grant agreement no. 316488 (KESTCELLS). The authors from IREC and IN^{2}UB belong to the M-2E (Electronic Materials for Energy) Consolidated Research Group and the XaRMAE Network of Excellence on Materials for Energy of the ''Generalitat de Catalunya''. E.S. thanks the Government of Spain for the ''Ramon y Cajal'' fellowship (RYC-2011-09212) and H. X. thanks support from the ''China Scholarship Council'' fellowship (CSC No. 201206340113). A.J.J. is funded by the EPSRC Doctoral Training Centre in Sustainable Chemical Technologies (EP/G03768X/1). A.W. acknowledges support from the Royal Society and the ERC (grant no. 277757). DFT calculations made use of UK national facility ARCHER, *via* A.J.J. and A.W.'s membership of the UK's HPC Materials Chemistry Consortium which is funded by EPSRC grant EP/L000202, and of the University of Bath's HPC facilities.

References

1 D. S. Patil and D. K. Gautam, *Phys. B*, 2004, **344**, 140–146.
2 S. A.-B. Nasrallah, S. B. Afia, H. Belmabrouk and M. Said, *Eur. Phys. J. B*, 2005, **43**, 3–9.
3 Y. Ichimura, K. Kishino, M. Satake, M. Kuramoto and A. Yoshida, *J. Cryst. Growth*, 1995, **150**(Part 2), 812–816.
4 H. Okuyama, E. Kato, S. Itoh, N. Nakayama, T. Ohata and A. Ishibashi, *Appl. Phys. Lett.*, 1995, **66**, 656–658.
5 Y. P. V. Subbaiah, P. Prathap, K. T. R. Reddy, D. Mangalaraj, K. Kim and J. Yi, *J. Phys. D: Appl. Phys.*, 2007, **40**, 3683.
6 S. V. Sorokin, S. V. Gronin, E. A. Evropeytsev, I. V. Sedova, A. A. Toropov and S. V. Ivanov, *J. Cryst. Growth*, 2015, **425**, 212–215, DOI: 10.1016/j.jcrysgro.2015.02.007.
7 S. Fridjine, S. Touihri, K. Boubaker and M. Amlouk, *J. Cryst. Growth*, 2010, **312**, 202–208.
8 H. Xie, M. Dimitrievska, X. Fontané, Y. Sánchez, S. López-Marino, V. Izquierdo-Roca, V. Bermúdez, A. Pérez-Rodríguez and E. Saucedo, *Sol. Energy Mater. Sol. Cells*, 2015, **140**, 289–298.
9 A. Fairbrother, L. Fourdrinier, X. Fontané, V. Izquierdo-Roca, M. Dimitrievska, A. Pérez-Rodríguez and E. Saucedo, *J. Phys. Chem. C*, 2014, **118**, 17291–17298.
10 P. Kannappan, K. Asokan, J. B. M. Krishna and R. Dhanasekaran, *J. Alloys Compd.*, 2013, **580**, 284–289.
11 P. Kannappan and R. Dhanasekaran, *J. Cryst. Growth*, 2014, **401**, 691–696.
12 L.-J. Chen, C.-R. Lee, Y.-J. Chuang, Z.-H. Wu and C. Chen, *CrystEngComm*, 2015, **17**, 4434–4438.
13 R. G. Valeev, E. A. Romanov, V. L. Vorobiev, V. V. Mukhgalin, V. V. Kriventsov, A. I. Chukavin and B. V. Robouch, *Mater. Res. Express*, 2015, **2**, 025006.
14 T. Basak, M. N. Rao, S. L. Chaplot, N. Salke, R. Rao, R. Dhanasekaran, A. K. Rajarajan, S. Rols, R. Mittal, V. B. Jayakrishnan and P. U. Sastry, *Phys. B*, 2014, **433**, 149–156.
15 G. L. Agawane, S. W. Shin, S. A. Vanalakar, A. V. Moholkar, K. V. Gurav, M. P. Suryawanshi, J. Y. Lee, J. H. Yun and J. H. Kim, *Mater. Res. Bull.*, 2014, **55**, 106–113.
16 H. K. Sadekar, A. V. Ghule and R. Sharma, *J. Alloys Compd.*, 2011, **509**, 5525–5531.
17 I. F. Chang and S. S. Mitra, *Phys. Rev.*, 1968, **172**, 924–933.
18 J. F. Scott, T. C. Damen, W. T. Silfvast, R. C. C. Leite and L. E. Cheesman, *Opt. Commun.*, 1970, **1**, 397–399.
19 S. S. Kumar, M. A. Khadar, K. G. M. Nair, S. Dhara and P. Magudapathy, *J. Raman Spectrosc.*, 2008, **39**, 1900–1906.
20 A. Fairbrother, V. Izquierdo-Roca, X. Fontané, M. Ibáñez, A. Cabot, E. Saucedo and A. Pérez-Rodríguez, *CrystEngComm*, 2014, **16**, 4120–4125.
21 M. Dimitrievska, A. Fairbrother, X. Fontané, T. Jawhari, V. Izquierdo-Roca, E. Saucedo and A. Pérez-Rodríguez, *Appl. Phys. Lett.*, 2014, **104**, 021901.
22 M. Placidi, M. Dimitrievska, V. Izquierdo-Roca, X. Fontané, A. Castellanos-Gomez, A. Pérez-Tomás, N. Mestres, M. Espindola-Rodriguez, S. López-Marino, M. Neuschitzer, V. Bermudez, A. Yaremko and A. Pérez-Rodríguez, *2D Mater.*, 2015, **2**, 035006.
23 J. Rodríguez-Carvajal, *Phys. B*, 1993, **192**, 55–69.
24 G. Kresse and J. Hafner, *Phys. Rev. B: Condens. Matter Mater. Phys.*, 1993, **47**, 558–561.
25 J. C. Jamieson and H. H. Demarest Jr., *J. Phys. Chem. Solids*, 1980, **41**, 963–964.

26 P. D. O. Madelung, *Semiconductors: Data Handbook*, Springer, Berlin Heidelberg, 2004, pp. 173–244.
27 J. P. Perdew, A. Ruzsinszky, G. I. Csonka, O. A. Vydrov, G. E. Scuseria, L. A. Constantin, X. Zhou and K. Burke, *Phys. Rev. Lett.*, 2008, **100**, 136406.
28 A. V. Krukau, O. A. Vydrov, A. F. Izmaylov and G. E. Scuseria, *J. Chem. Phys.*, 2006, **125**, 224106.
29 J. Baars and G. Brandt, *J. Phys. Chem. Solids*, 1973, **34**, 905–909.
30 Y. Matsushima, K. Yoshino, Y. Yamamoto, S. R. Tiong and M. Hiramatsu, *J. Cryst. Growth*, 1992, **117**, 328–330.
31 O. Senthil Kumar, S. Soundeswaran and R. Dhanasekaran, *Mater. Chem. Phys.*, 2004, **87**, 75–80.
32 O. Senthil Kumar, S. Soundeswaran, D. Kabiraj, D. K. Avasthi and R. Dhanasekaran, *J. Cryst. Growth*, 2005, **275**, e567–e570.
33 J. Tauc and A. Menth, *J. Non-Cryst. Solids*, 1972, **8–10**, 569–585.
34 S. Park, H. Kim, C. Jin and C. Lee, *Curr. Appl. Phys.*, 2012, **12**, 499–503.
35 W. G. Nilsen, *Phys. Rev.*, 1969, **182**, 838–850.
36 W. Taylor, *Phys. Lett. A*, 1967, **24**, 556–558.
37 E. A. Vinogradov, B. N. Mavrin, N. N. Novikova, V. A. Yakovlev and D. M. Popova, *Laser Phys.*, 2009, **19**, 162–170.
38 M. Dimitrievska, A. Fairbrother, E. Saucedo, A. Pérez-Rodríguez and V. Izquierdo-Roca, *Appl. Phys. Lett.*, 2015, **106**, 073903.
39 K. Hayashi, N. Sawaki and I. Akasaki, *Jpn. J. Appl. Phys.*, 1991, **30**, 501.
40 J. Lu, H. Liu, C. Sun, M. Zheng, M. Nripan, G. S. Chen, G. M. Subodh, X. Zhang and C. H. Sow, *Nanoscale*, 2012, **4**, 976–981.
41 M. Dimitrievska, A. Fairbrother, A. Pérez-Rodríguez, E. Saucedo and V. Izquierdo-Roca, *Acta Mater.*, 2014, **70**, 272–280.
42 *Raman Scattering in Materials Science*, ed. W. H. Weber and R. Merlin, Springer Berlin Heidelberg, Berlin, Heidelberg, 2000, vol. 42.
43 P. Yu and M. Cardona, *Fundamentals of Semiconductors: Physics and Materials Properties*, Springer Science & Business Media, 2010.
44 J. E. Bernard and A. Zunger, *Phys. Rev. B: Condens. Matter Mater. Phys.*, 1987, **36**, 3199–3228.
45 S.-H. Wei and A. Zunger, *J. Appl. Phys.*, 1995, **78**, 3846–3856.
46 Y.-H. Li, A. Walsh, S. Chen, W.-J. Yin, J.-H. Yang, J. Li, J. L. F. D. Silva, X. G. Gong and S.-H. Wei, *Appl. Phys. Lett.*, 2009, **94**, 212109.
47 M. Dimitrievska, H. Xie, A. Fairbrother, X. Fontané, G. Gurieva, E. Saucedo, A. Pérez-Rodríguez, S. Schorr and V. Izquierdo-Roca, *Appl. Phys. Lett.*, 2014, **105**, 031913.
48 M. Dimitrievska, G. Gurieva, H. Xie, A. Carrete, A. Cabot, E. Saucedo, A. Pérez-Rodríguez, S. Schorr and V. Izquierdo-Roca, *J. Alloys Compd.*, 2015, **628**, 464–470.

